ADVANCED HEALTHCARE MATERIALS
www.advhealthmat.de

Woven Electroanalytical Biosensor for Nucleic Acid Amplification Tests

Shirin Khaliliazar, Ingrid Öberg Månsson, Andrew Piper, Liangqi Ouyang, Pedro Réu, and Mahiar Max Hamedi**

Fiber-based biosensors enable a new approach in analytical diagnostic devices. The majority of textile-based biosensors, however, rely on colorimetric detection. Here a woven biosensor that integrates microfluidics structures in combination with an electroanalytical readout based on a thiol-self-assembled monolayer (SAM) for Nucleic Acid Amplification Testing, NAATs is shown. Two types of fiber-based electrodes are systematically characterized: pure gold microwires (bond wire) and off-the-shelf plasma gold-coated polyester multifilament threads to evaluate their potential to form SAMs on their surface and their electrochemical performance in woven textile. A woven electrochemical DNA (E-DNA) sensor using a SAM-based stem-loop probe-modified gold microwire is fabricated. These sensors can specifically detect unpurified, isothermally amplified genomic DNA of *Staphylococcus epidermidis* (10 copies/µL) by recombinase polymerase amplification (RPA). This work demonstrates that textile-based biosensors have the potential for integrating and being employed as automated, sample-to-answer analytical devices for point-of-care (POC) diagnostics.

1. Introduction

Fibrous materials, such as threads, paper, and fabrics, have been extensively used over the past decades as substrates for microfluidics to enable bioanalytical point-of-care (POC) devices.[1] Fiber-based materials offer two main advantages to microfluidic systems: i) they allow passive fluid transport through wicking, thus eliminating the need for auxiliary pumping equipment; and ii) their surface is printable allowing for mass production of the electronic, fluidic, and biological functions through printing. These important features considerably reduce the fabrication complexity eliminating the need for microfabrication or multistep processes.[2]

One mode of biosensing, particularly interesting in fiber-based POC analytical devices, is electroanalytical detection due to its high sensitivity and specificity, and its capability to be readily incorporated in electrodes that perform the sensing into fibrous materials through printing.[3] Additionally, using low-cost, portable electronics enables digital on-site[2c] readout and connection to the cloud,[4] thus eliminating the need for advanced optical instruments for detection.

The performance of electroanalytical biosensors is considerably linked to the choice of electrode materials.[5] Carbon electrodes are the most typical electrodes in fiber-based electroanalytical devices: they are low-cost and easy to integrate into devices using inkjet-printing, pencil-drawing, screen-printing, and weaving.[3b,6] Functionalized helical fiber bundles of carbon-nanotube as an implanted electrochemical sensor, enabled wireless real-time monitoring of physiological signals.[7] Carbon paste and inks, however, suffer from high resistance as they contain non-conductive polymeric binders.[8] More importantly, carbon electrodes are not generally suitable for the fabrication of self-assembled monolayer (SAM)-based electrochemical biosensors. SAMs offer sensitive, quantitative electrical responses, which make them ideal for point-of-care applications. Thiol-based SAMs are extensively used due to their ease of fabrication through chemisorption of highly reactive thiol groups onto clean gold electrode surfaces, which are then directly used as working electrodes in electrochemical measurements.[9] SAMs are difficult to integrate using printing techniques because clean gold surfaces cannot easily be printed and necessitate multistep complex and tedious chemical modifications to be immobilized on printed carbon supports.[10] Despite the number of reports on thiol SAM-based electrochemical sensors for detection of DNA or other biological analytes, there is still a lack of SAM-based electrochemical biosensors for fiber-based and other high throughput point-of-care diagnostics.[11]

Gold microwires present an interesting alternative to carbon-printed electrodes for electrochemical fiber-based analytical devices,[12] because many types of gold microwires are available in pure and alloyed compositions and the 1D structure gives unprecedented flexibility and mechanical integrity to normally rigid planar electrodes.[10a,13] Fosdick et al. reported the first SAM-modified gold microwire electrodes integrated into a hallow channel of a paper-based microfluidic device to perform electrochemistry in bulk solution under laminar flow conditions in

S. Khaliliazar, I. Öberg Månsson, Dr. A. Piper, Dr. L. Ouyang, Dr. P. Réu, Prof. M. M. Hamedi
Department of Fibre and Polymer Technology
School of Engineering Sciences in Chemistry, Biotechnology and Health
KTH Royal Institute of Technology
Tekninkringen 56-58, Stockholm, SE-100 44, Sweden
E-mail: liangqi@kth.se; mahiar@kth.se

The ORCID identification number(s) for the author(s) of this article can be found under https://doi.org/10.1002/adhm.202100034

DOI: 10.1002/adhm.202100034

single layer paper-based devices.[12] Besides this work, very little attention has been given to integrating microwire and thread-based sensors for electrochemical textile-based diagnostic devices.[14]

Here we present a woven micro total analysis system (μTAS)[1b,15a,15b] and use it as a DNA biosensor. These devices were fabricated by first forming SAM on gold surfaces, including pure-gold microwires as well as plasma coated gold multifilament threads, and further weaving these fiber electrodes into textiles to create advanced 3D-microfluidic devices. We selected Coolmax yarn, twisted continuous filaments of polyester that is engineered to wick moisture, as an inlet and a wicking channel to enable spontaneous liquid to flow without the need for external pumps and with a high flow rate.[12,16]

2. Results and Discussion

We systematically studied the electrochemical performance of unmodified and SAM-modified-gold microwires and gold multifilament threads before and after weaving, to investigate the best mode of integration into textiles. Finally, as proof of concept, we integrated a stem-loop (S-L) DNA probe-modified gold microwire to detect unpurified recombinase polymerase amplification (RPA) products[17] in the woven μTAS devices.

2.1. Woven Fiber Electrodes Characterization

In this study we employed two different types of fiber electrodes: i) monofilament gold microwires, commonly found as bond wires in microelectronics, which are readily available in small dimensions (100 µm diameter, 99.99% purity) and are flexible to weave; and ii) multifilament polyester (PET) threads (246 µm diameter), plasma coated with gold. The gold multifilament threads benefit from wicking property, electrical conductivity, and more importantly the possibility of biofunctionalizing the surface without the need for any pre-cleaning or modifications. These off-the-shelf fiber electrodes can be chemically functionalized[15b,17] and are therefore better alternatives to the fabrication of conductive gold fibers that require uniform and thin deposition of the metal on the fiber substrates, which is not easily achievable at the lab scale.[18]

We used these fiber electrodes for the formation of self-assembled monolayers as shown schematically in **Figure 1A**,B. To assess the formation of SAMs we self-assembled 6-mercapto-1-hexanol (6MCH) on the gold microwires and the gold multifilament threads. We conducted cyclic voltammetry at different scan rates (10 mV s^{-1} -300 mV s^{-1}) in 5 mmol L^{-1} of potassium ferricyanide $K_3[Fe(CN)_6]$ solution before and after incubation of the electrodes in 1 mmol L^{-1} 6MCH solution overnight, (Figure S1, Supporting Information).

We calculated the electrochemical effective surface area of the gold microwires and gold multifilament threads, using the Randles–Sevcik equation, (Equation (1)):

$$i_p = (2.69 \times 10^5) n^{3/2} D^{1/2} C A \nu^{1/2} \quad (1)$$

where n is the number of transferred electrons for the redox reaction, which is one for $Fe(CN)_3{}^{-6}$ according to the following half-reaction (Equation (2)), D is the diffusion coefficient (6.70×10^{-6} cm^2 s^{-1}), C is the molar concentration of ferricyanide solution (5 mmol L^{-1}), ν is the scan rate (V s^{-1}), and A is the effective surface area (cm^2), which we calculated for the electrodes:

$$Fe(CN)_6^{3-} + e^- \rightarrow Fe(CN)_6^{4-} \quad (2)$$

The clean gold microwires and off-the-shelf (unmodified) gold multifilament threads had an effective surface area of 2.7 ± 0.2 mm^2 and 7 ± 3.8 mm^2, respectively. Both electrodes indicated a linear correlation between oxidation peak current (i_p) of redox molecules versus the square root of scan rates ($\nu^{1/2}$) in the Randles–Sevcik equation as seen in Figure 1D. This verifies the electrochemically reversible electron transfer process, which results from a fast electron transfer between the redox molecules and the electrode surface, (for complete CV data see Figure S1, Randles–Sevcik plots see Figures S7 and S8, and for the accordingly calculated effective surface see Figure S6, Supporting Information).

After overnight incubation in 1 mmol L^{-1} 6MCH solution, the gold microwires and the gold multifilament threads did not show any redox peaks in ferricyanide/ferrocyanide solution, Figure 1C, thus confirming the formation of a densely packed SAM on the surface of the electrodes, which inhibited the electrochemical redox reaction of the redox molecules at the electrode interface in the solution.

We next designed a woven textile to integrate the gold fiber electrodes along with other analogous wire/thread as counter and pseudo reference electrodes to achieve a three-electrode textile microfluidic electroanalytical device, see schematic **Figure 2A**.

We used the SAM-modified gold microwires and gold multifilament threads as working electrodes. We wove gold microwires/plasma gold-coated threads as counter and silver microwires/plasma silver-coated polyester threads as pseudo reference electrodes. Figure 2D,E shows the photos of the real Coolmax-cotton woven microfluidic devices with integrated microwire and thread fiber electrodes being loaded with ferricyanide solution, respectively.

To fabricate the woven microfluidic device we used Coolmax yarn, engineered polyester filaments with hexachannel cross-section, which cause quick-moisture wicking.[19] Polyester as synthetic fiber does not absorb liquids and merely transfers liquids through the hallow area between and along the filaments created by the hexachannel cross-sections, Figure 2F. Therefore, we employed Coolmax yarn to eliminate the adsorption of liquids in the wicking yarns throughout the electrochemical measurement.

The integration of the textile microfluidic structure enables the delivery of the solution to the fiber-based electrodes, for electroanalytical detection. Here the interface between the Coolmax yarns and the fiber electrodes creates the electrochemical detection zone. To maximize the supply of solution at the interface between the Coolmax yarns and the SAM-modified working electrodes, we designed a weave, in which the wicking channels were both vertical (in the wrap) and horizontal (in the weft) to the fiber electrodes. We used sewing cotton yarns, which had a thin layer of wax as passive yarns to frame the weave.

To evaluate the electrochemical performance of the integrated fiber electrodes in the woven microfluidic device, we conducted systematic electrochemical studies using cyclic voltammetry

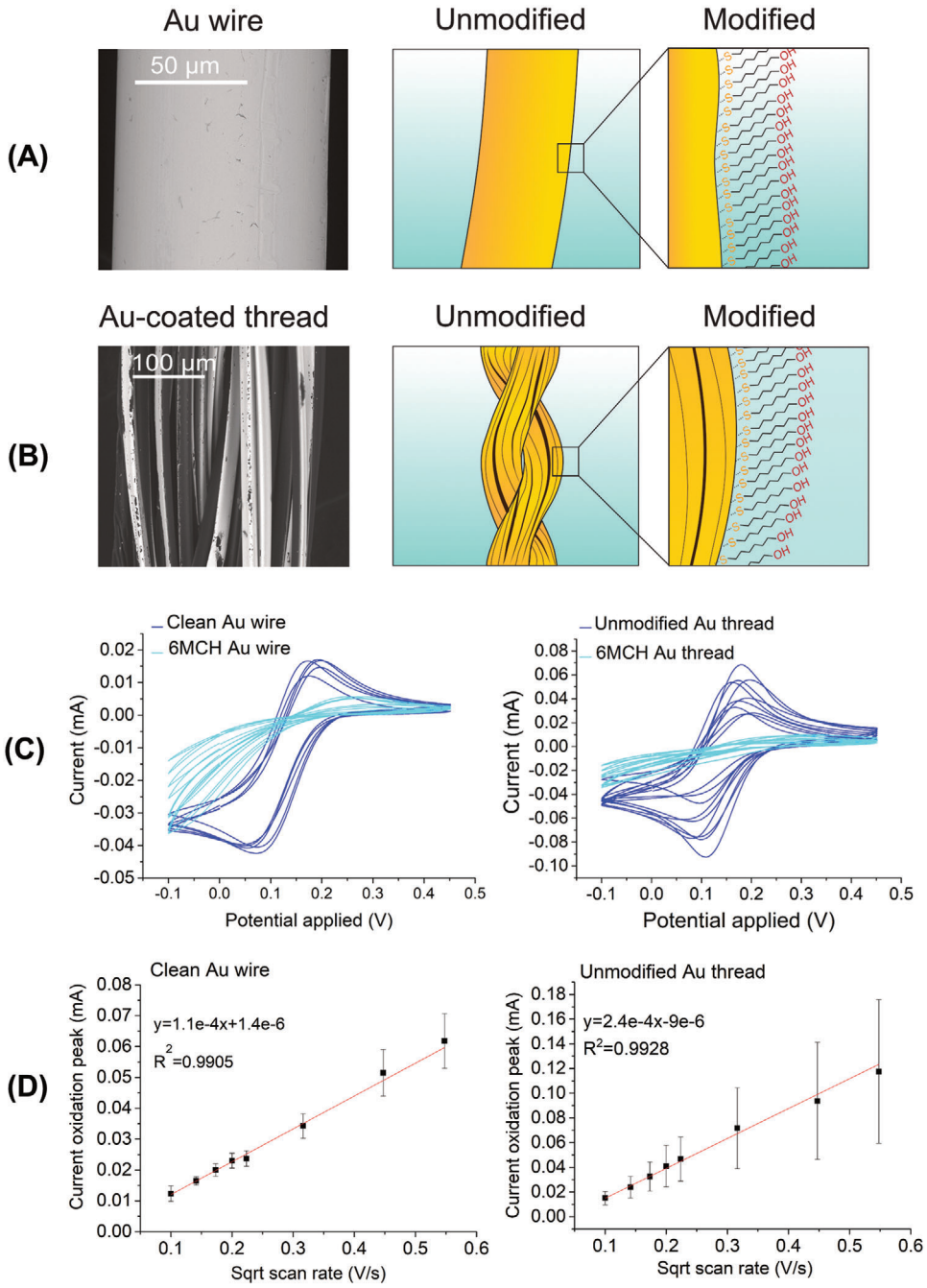

Figure 1. Characterization of the gold microwires and the plasma gold-coated polyester multifilament threads A) scanning electron microscopy (SEM) image of the gold microwire and schematic of the SAM-modified Au microwire by 6-mercapto-1-hexanol (6MCH). B) SEM image of the plasma gold-coated polyester multifilament threads and schematic of the SAM-modified Au threads by 6-mercapto-1-hexanol (6MCH). C) Cyclic voltammograms of clean ($n = 5$) and 6MCH-modified gold wires ($n = 9$) along with cyclic voltammograms of unmodified ($n = 9$) and 6MCH-modified gold threads ($n = 7$). Cyclic voltammograms were recorded in 5 mmol L^{-1} of potassium ferricyanide at a scan rate of 50 mV s^{-1} versus Ag microwires and Ag threads as pseudo-reference electrodes. D) Randles–Sevcik plots of the clean Au wires ($n = 5$) and the off-the-shelf and unmodified gold multifilament threads ($n = 9$) in potassium ferricyanide solution. Data points represent mean ± SD.

(10–300 mV s^{-1} scan rates) for unmodified and 6MCH-modified gold microwires and threads in three sequential steps as shown in Figure 2A: i) we characterized the electrodes in a 5 mmol L^{-1} of potassium ferricyanide solution; ii) we wove these fiber electrodes into the woven microfluidic device together with Coolmax yarns as wicking channels and measured CVs by directly connecting the textile fiber electrodes to a potentiostat and, adding 100 µL potassium ferricyanide solution (5 mmol L^{-1}) to the Coolmax inlet channels; and iii) we removed the electrodes out of the weave, to reanalyze them in the redox solution.

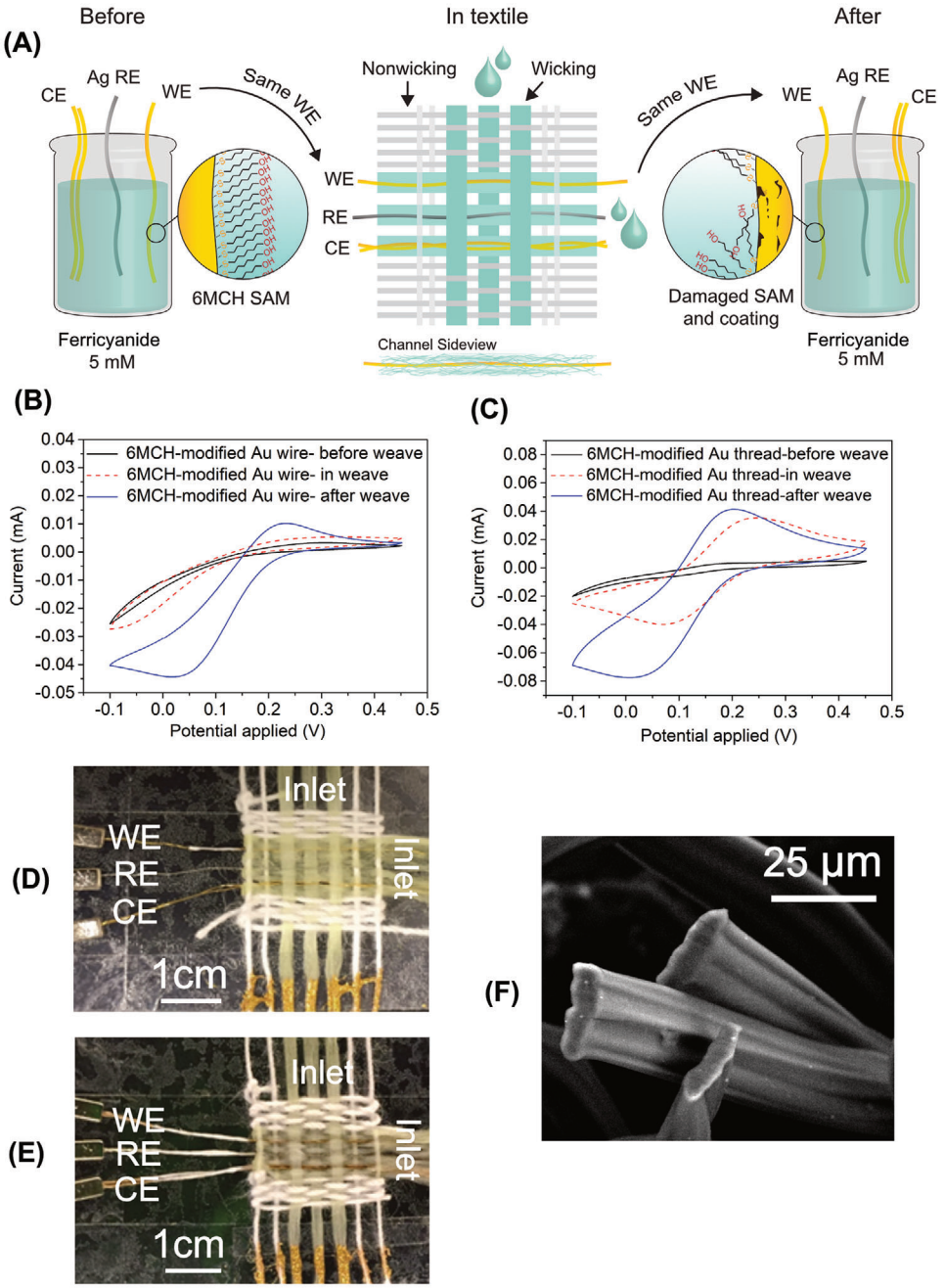

Figure 2. Electrochemical characterization of 6-mercapto-1-hexanol (6MCH)-modified gold microwires and plasma coated gold multifilament threads A) schematics of stepwise-electrochemical characterization of 6MCH-modified gold microwires and threads: i) before weaving the electrodes into Coolmax weave; ii) in the weave; and iii) after taking them out of the weave. (B) and (C) cyclic voltammograms of the 6MCH-modified gold microwire and the thread in the aforementioned three-stepwise condition, respectively in 5 mmol L^{-1} of potassium ferricyanide at a scan rate of 50 mV s^{-1} versus an Ag microwire and an Ag thread as pseudo-reference electrodes. (D) and (E) photos of the real integrated microwires and gold multifilament threads into the woven microfluidic devices, respectively. F) Scanning electron microscopy (SEM) image of the Coolmax yarn cross-section.

The 6MCH-modified Au threads in the weave showed an effective surface area of 3.6 ± 2.6 mm^2. This value increased by 2-fold to 6.5 ± 2.7 cm^2 after taking the modified threads out of the weave, **Table 1**.

The increase of the effective surface area of the modified gold threads in the weave and after taking them out of the weave indicates damaging or scratching of a part of the SAM on the electrodes' surface, during the weaving and handling of the electrodes.[20] The presence and increment of the redox peak currents in cyclic voltammograms of the 6-MCH modified gold thread as seen in Figure 2C, clearly verify the formation of the uncovered area on the electrode surface in the weave and after removing them from the weave, (Figures S2 and S3, Supporting Information, show CV scans for the gold

Table 1. Calculated uncovered electrochemical effective surface area (measured in 5 mmol L^{-1} of potassium ferricyanide solution), for 15 mm long clean gold microwires ($n = 5$), 6MCH-modified microwires ($n = 9$), off-the-shelf unmodified gold multifilament yarn ($n = 9$), and 6-MCH modified gold multifilament yarn ($n = 7$). Results are expressed as mean ± SD.

Uncovered electrochemical effective surface area [mm^2]				
		6MCH-modified		
Fiber electrode	Unmodified	Before weave	In weave	After weave
Au wire	2.7 ± 0.2	Densely packed SAM-surface	Densely packed SAM-surface	1.4 ± 0.9
Au thread	7± 3.8	Densely packed SAM-surface	3.6 ± 2.6	6.5 ± 2.7

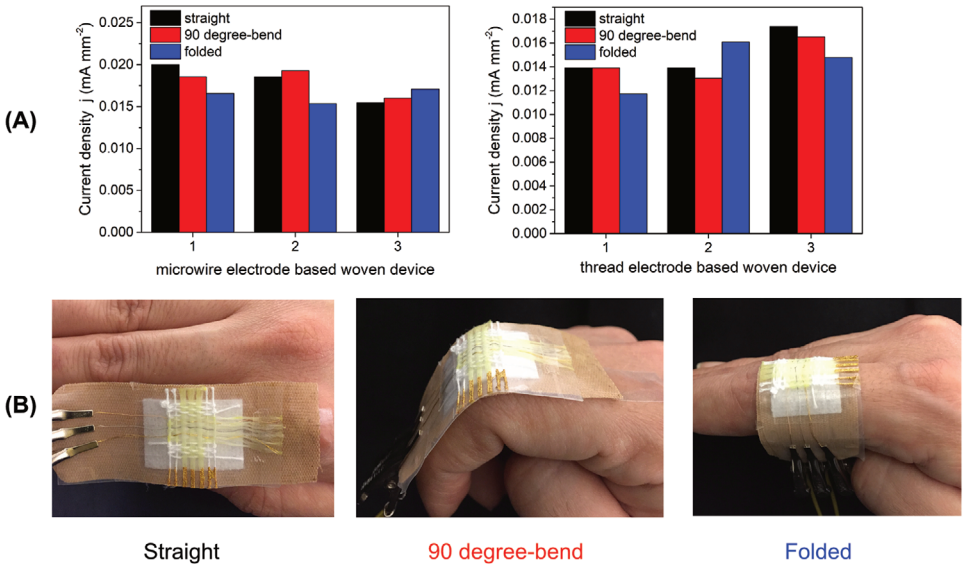

Figure 3. Flexibility characterization of the woven devices including off-the-shelf thread ($n = 3$) and microwire electrodes ($n = 3$), attached to a figner of a human subject, at three different conditions: straight, 90 degree-bend and folded form A) current densities of the woven fiber electrodes into the microfluidic device which is the ratio of the oxidation peak current of potassium ferricyanide (in respective CV scans) to the effective surface area of the fiber-electrodes' B) photos of the real woven microfluidic devices in the straight, 90 degree-bend and folded conditions.

multifilament thread electrodes in this three-step characterization).

Similarly, we calculated the effective surface area of the clean (electropolished) microwires during the three different steps, Table 1. In the first step, we were unable to calculate the effective surface area for the modified gold microwires densely packed by SAM on the surface, which prevented redox reaction at the interface. In step (ii), when we wove the modified gold microwires into the Coolmax weave, only three out of nine wires indicated redox peaks in CVs, which did not show the linear correlation in the Randles–Sevcik equation. In step (iii), when we removed the modified wires of the weave we obtained an effective surface area of 1.4 ± 0.9 mm^2 for four out of nine microwires, (Figures S4, S5, and S8, Supporting Information). Figure 2B shows the redox peaks for the 6-MCH modified Au wire, which indicates the available uncovered electrochemical surface area after taking that out of the weave. This increase in the surface area could be attributed to damaged SAM on the microwire surface, caused by scratching. Additionally, scanning electron microscope (SEM) images of unmodified gold microwires and gold plasma coated PET multifilament threads in Figure 1A,B, show inherent defects on their surfaces. These defects, which are more remarkable on the gold multifilament threads' surface than that of microwires can differently affect the SAM formation on gold surfaces and this could be extended by handling and integrating into the weave.

Gold multifilament threads offer almost three times higher effective surface area than gold microwires, and SAM can be formed on their surfaces without the need for a pre-cleaning step. The measured effective surface areas in Table 1 however, indicated that that the gold multifilament threads are more vulnerable to applied mechanical tensions during the weaving process than the modified gold microwires.

As flexibility is one of the important features of fiber-based biosensors, we characterized, therefore, our woven microfluidic device by fabricating them onto adhesive bandages (**Figure 3B**). We conducted cyclic voltammetry for the different woven devices in straight, 90 degree-bend, and folded form, as they were attached to a finger of a human subject. The results showed that both thread and microwire electrode-based woven devices preserved their electrochemical performance in different forms, as shown by the measured currents densities (Figure 3A and Figure S9, Supporting Information). Statistical *t*-tests (Table S1, Supporting Information) confirm the flexibility of the woven microfluidic devices and show no significant statistical difference

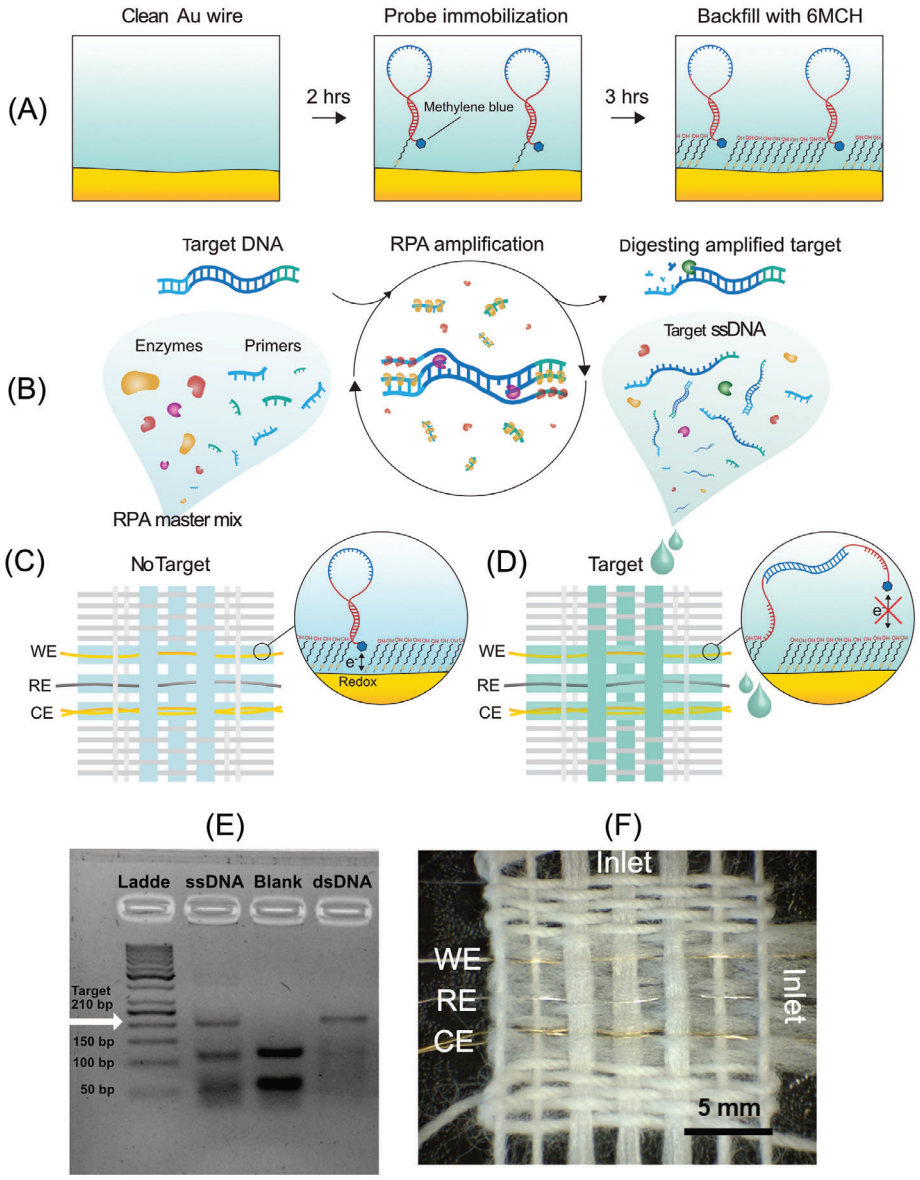

Figure 4. Schematics of E-DNA sensor fabrication, integration into the Coolmax-weave, and isothermal amplification RPA. A) Schematics of immobilization of methylene blue conjugated stem-loop (S-L) DNA probes on the clean gold microwire surface and later backfilling of the electrode surface by 6MCH. B) Schematics of the mechanism of recombinase polymerase amplification (RPA) and providing ssDNA target using lambda exonuclease enzyme for the detection step. (C) and (D) schematics of the woven E-DNA sensor into Coolmax-cotton weave, including a stem-loop (S-L) DNA probe modified-gold microwire, a silver microwire, and double-gold microwires as working (WE), pseudo-reference (RE), and counter (CE) electrodes, in absence and presence of RPA target sample. E) Gel electrophoresis image of RPA amplified S. epidermidis genomic DNA with a target size of 210 bp, before converting to single-stranded DNA using exonuclease lambda enzyme as dsDNA product and after digesting the untargeted strand as ssDNA. F) Photo of the real E-DNA sensor integrated into the woven microfluidic devices.

in the measured current density of the fiber electrodes at different bending conditions.

In summary, these studies showed the flexibility and robustness of the woven microfluidic devices for on-body electroanalytical measurements. We could successfully coat both gold-microwires wires and plasma gold-coated threads with SAM-layers, but that the SAMs on the monofilaments were less sensitive for integration into woven devices. We, therefore, chose to use gold microwires to demonstrate an electroanalytical device for nucleic acid amplification testing, NAATs.

2.2. Integrating E-DNA Sensor into Woven Microfluidic Device

We chose a SAM-based stem-loop (S-L) DNA probe to fabricate an electrochemical DNA (E-DNA) sensor and integrate it into a textile μTAS. We modified the electropolished-gold microwires with 1 µM of the stem-loop DNA probe, **Figure 4A** illustrates the schematics of the SAM-(stem-loop) DNA probe-modified Au microwire. CV scans of the modified electrode confirmed the formation of methylene blue bonded-SAM on its surface, (Figure S10, Supporting Information). The 3′ terminus of the probe sequence

Table 2. Designed the RPA forward, reverse primers, and stem-loop (S-L) probe for S. epidermidis ATCC 12228.

RPA Forward-primer	5′-phosphate-TATAGGCTTAATTATCTCTGTTTTAG GAGCTT-3′
RPA Reverse-primer	5′-TGATAGGCACTATCTGTAAACAACATACTAAT-3′
Stem-loop (S-L) probe	5′MeBIN/GCGAGGAAGCTCCGGTCAACGCTTCC TCGC/3′ThioMC3-D

was modified with a thiol group to enable the spontaneous formation of the self-assembled monolayers of the stem-loop DNA probe on the gold microwires. The 5′ terminus of the probe was labeled with a methylene blue (MB) redox reporter, **Table 2**. Upon hybridization with the complementary DNA sequence, the probe undergoes a conformational change that moves the methylene blue further away from the electrode surface reducing the electrochemical current as shown schematically in Figure 4C,D. The E-DNA sensor showed a linear response in presence of 0.2–1 μM of the synthetic target sequence in solution with a technical limit of detection (LOD) of 0.5 μM.[17]

In a NAAT, the extracted nucleic acid (DNA/RNA) from bacterial or viral samples has to be amplified to provide detectable copies of target genes. Considering the potential of woven-based-E-DNA sensors for point-of-care diagnostics, we employed an isothermal amplification technique, RPA to make this system applicable for further bedside-testing. RPA works at a relatively low-constant temperature (37–42 °C) using recombinase enzyme, which forms a complex with forward and reverses primers and then hybridizes to the homologous sequence in the target DNA template.[21] Subsequently, the polymerase enzyme starts extending the primers in both strands through a strand displacement mechanism by thermostable, ssDNA binding-proteins (SSB) as shown schematically in Figure 4B.

We used *Staphylococcus epidermidis* as a model organism for methicillin-resistant *Staphylococcus aureus* (MRSA).[22] Despite *S. epidermidis* being classified as a biosafety level one (BSL-1) bacteria, some strands of it are known as a source of nosocomial infections, forming biofilms on implanted plastic devices such as dialysis catheters. Therefore,[23] its diagnosis is of some medical value.

We carried out RPA amplification for 10 copies of extracted genomic DNA of *S. epidermidis* as target samples and used the same master mix without DNA template as blank samples. Afterward, we used the exonuclease lambda enzyme to digest the non-target DNA strand as shown in Figure 4B and kept the target ssDNA complementary to the loop part of the stem-loop (S-L) DNA probe. Figure 4E shows the gel electrophoresis image of the RPA amplified *S. epidermidis* genomic DNA with a target size of 210 base pairs (bp) for the double-stranded DNA (dsDNA), and single-stranded DNA (ssDNA) obtained after digesting the untargeted strand by exonuclease lambda enzyme. The RPA blank sample contained all the components of the target sample master mix except the gDNA template, in which we instead used nuclease-free water. The ssDNA shows a band slightly lower than dsDNA, which could be due to the higher electromobility of ssDNA in the electric field than dsDNA.[24]

To integrate the E-DNA sensor into the woven device (with both vertical and horizontal wicking channel structure), we wove the stem-loop DNA probe-modified gold microwire as a working electrode, bare gold microwires as counter electrodes, and silver microwires as a pseudo-reference electrode. We chose this woven structure as it showed the most consistent flow behavior and allowed maximum liquid contact between the microwire electrodes and the wicking yarns (for more detailed information see Figure S11, Supporting Information). Figures 4C and 4D illustrate the schematic of the woven-based E-DNA sensor before and after adding target ssDNA to the weave and Figure 4F shows a photo of the real integrated E-DNA sensor.

We investigated the performance of the stem-loop DNA probe-functionalized microwires in woven textiles by adding 60 μL of the unpurified RPA samples to the Coolmax inlets of the weave. First, we added PBS (1×, pH 7.4), waited for 5 min, and performed square wave voltammetry (SWV), to obtain a baseline for the stem-loop DNA probe, and then dried the inlets. Next, we introduced either a 250-fold diluted, unpurified RPA blank treated with exonuclease lambda enzyme, or ssDNA RPA target amplicon (10 copies/μL *S. epidermidis* DNA template, which was 50 copies/reaction), to the wicking inlets of the weave. We measured the stem-loop DNA probe response to the RPA products after 5 min of hybridization by SWV technique for four separate, integrated weaves for either of the RPA products: blank, **Figure 5B** and target, Figure 5C (Figures S13 and S14, Supporting Information, show the SWV scans of the four separate woven E-DNA sensors).

To further investigate the DNA probe performance, we characterized the SWV response of the integrated E-DNA sensor to PBS (1×) with 5 min measurement intervals for six individual woven-based E-DNA sensors as seen in Figure 5A and Figure S12, Supporting Information.

Figure 5D illustrates the signal suppression of the four separate woven electrochemical DNA sensors tested for RPA target or RPA blank samples. It indicates an average of 68% decrease in peak current in SWV scans in presence of ssDNA RPA target amplicon; whereas the RPA blank, as the negative control shows a 47% drop of the signal along with 27% signal suppression for PBS after 5 min. According to the statistical results (see *t*-test statistics in Table S3, Supporting Information), the integrated stem-loop DNA probe-labeled gold microwire in the weave is specific to the samples without any DNA (pure PBS buffer), negative control sample (RPA blank sample containing non-specific amplicons), and RPA target product (with an initial 10 copies/μL *S. epidermidis* purified genomic DNA) and can detect these three samples specifically. The signal suppression higher than 56% in the woven E-DNA sensor after 5 min of hybridization is indicative of a positive test result. The limit of the detection of the whole system is 10 copies/μL lower than most of the previous reports; RPA amplifies as few as 10 copies/μL of *S. epidermidis* genomic DNA.[25] The total assay time for amplification and detection is 65–70 min.

3. Conclusion

Here we used SAM modified-microwires to fabricate woven E-DNA sensors. We presented the two types of off-the-shelf gold fiber: gold monofilament microwires (bond wires) and plasma

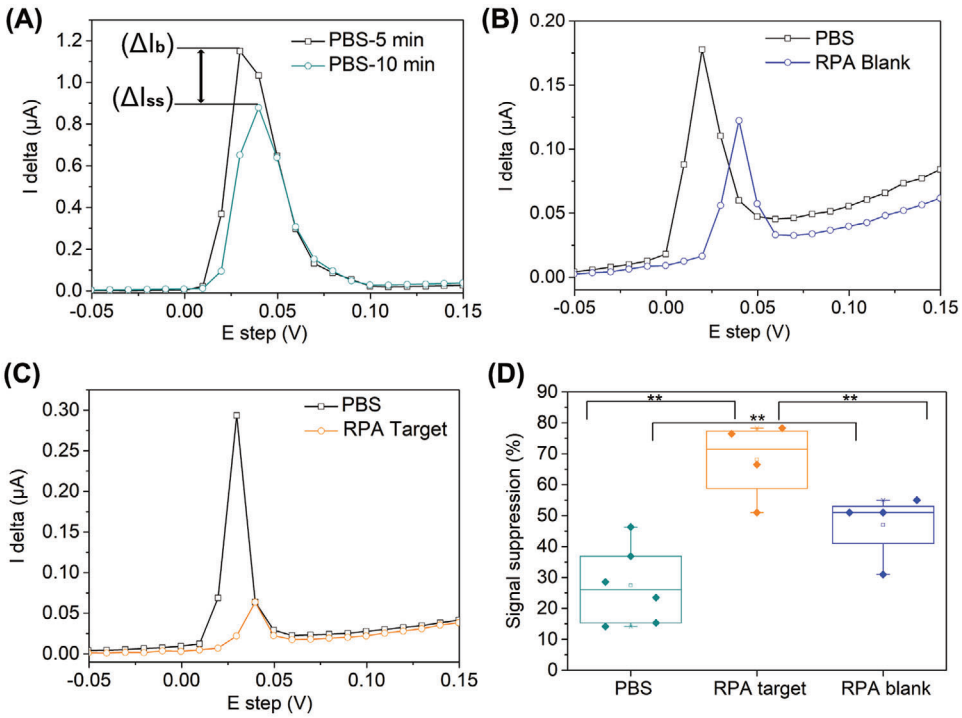

Figure 5. Detecting RPA products through woven E-DNA sensors into the Coolmax-cotton weave using signal suppression ($SS = (\Delta Ib - \Delta Iss) / \Delta Ib$)), in which ΔIb is the baseline peak current and ΔISS is the suppressed peak current. A) Typical SWV scans of the woven E-DNA sensor for added 60 µL of 1× PBS (pH 7.4) after 5 min. (B) Typical SWV scans of the woven E-DNA sensor for added 60 µL of unpurified 250-fold diluted RPA blank (treated by lambda exonuclease enzyme) product as a negative control sample after 5 min of hybridization. C) Typical SWV scans of the woven E-DNA sensor for added 60 µL of unpurified 250-fold diluted ssDNA RPA target product after 5 min of hybridization. D) Signal suppression of the integrated E-DNA sensors into the woven devices in presence of the unpurified RPA amplified ssDNA target (with an initial 10 copies/µL of *S. epidermidis* genomic DNA), the RPA blank product treated with lambda enzyme and PBS (1×, pH 7.4) after 5 min of hybridization. Reported data are based on the independent woven E-DNA sensors ($n = 4$) for RPA products and ($n = 6$) for PBS (1×, pH 7.4). Statistical analysis is carried out using Student's *t*-test (two-tailed) and ** $p < 0.05$ is considered significant.

gold-coated multifilament polyester threads which are inert, conductive, flexible, biocompatible, and chemically functionalizable microelectrodes for fabricating SAM-based biosensors. We think these are important criteria when selecting proper fiber electrodes for textile-based biosensors..[26] The woven microfluidic devices took advantage of the wicking property of the wicking yarns, to transfer liquids to the surface of the microwires/multifilament threads, which acted as electrodes to enable electroanalytical devices. The SAM-modified gold multifilament threads were, however, more vulnerable to weaving, which resulted in higher loss/damage of the SAM on the electrodes' surfaces. We performed a nucleic acid amplification test (NAAT), by combining the woven E-DNA sensor with an isothermal amplification method (RPA) that works at low temperatures (37–42 °C). These woven sensors could specifically detect unpurified and isothermally amplified *S. epidermidis* genomic DNA (10 copies/µL concentration). The limit of the detection of the whole system is 10 copies/µL with a total assay time of 65–70 min. In summary, we show the possibility to weave μTAS systems that enable NAATs with electrical readout. We think these kinds of textile-based sensors have the potential to be produced at scale, using textile manufacturing techniques, and find use in wearable sensors and point-of-care diagnostics.[26,27]

4. Experimental Section

Materials: We purchased gold wire, (100 µm diameter, 99.99% trace metals basis), silver wire (100 µm diameter, 99.99% trace metals basis), tris (2-carboxyethyl) phosphine hydrochloride (TCEP), 6-mercapto-1-hexanol (6-Hydroxy-1-hexanethiol, 97%), and sulfuric acid (99.999%) from Sigma-Aldrich (Sweden). We purchased gold and silver multifilament threads from Swicofil (SWICOFIL AG, Switzerland) and Coolmax yarn from Invista (UK), see Table S2, Supporting Information, for the specification of all the yarns and threads. *S. epidermidis* ATCC 12228 was purchased from ATCC LGC Standards (USA). we used QIAamp DNA kit (QIAGEN, Germany) for extraction and purification of genomic DNA of *S. epidermidis* after inoculation in the lab. The TwistAmp Basic RPA kit and Oligonucleotide primers were purchased from TwistDX Limited (Cambridge, UK) and Eurofins Genomics Europe Shared Services GmbH (Germany), respectively. Stem-loop oligonucleotide probe was customized by Integrated DNA Technologies, Inc. (IDT, Iowa, USA). Lambda exonuclease enzyme, phosphate-buffered saline (PBS) tablets pH 7.4, nuclease-free water, and 10× Tris-borate-EDTA (TBE) buffer were purchased from Fisher Scientific (Sweden).

Electrochemical Measurements: We conducted all electrochemical measurements using Autolab PGSTAT204N with MUX 16 module (Metrohm Autolab, Sweden) through the accompanying NOVA 1.11 software package.

SAM-Modification of Gold Microwires and Gold Threads: We modified the clean gold microwires, which were beforehand electropolished in 0.5 M sulfuric acid solution from (−400 to 1350 mV) versus Pt reference and

counter electrodes at a rate of 100 mV s^{-1} until the CV stabilized,[28] and the off-the-shelf gold thread overnight in 1 mmol L^{-1} of 6-Mercapto-1-hexanol (6MCH) solution made in ethanol in the dark at room temperature. We thoroughly rinsed the modified wires and threads using ethanol and MQ-water, respectively. We defined the geometric area, 15 mm length, for unmodified and modified threads and microwires using a nail polish, which also helped to stop the liquid flow in the gold threads toward the clamping contact to the Autolab potentiostat.

Gold Microwires and Threads Characterization in Bulk and Woven Textile: We characterized the modified and unmodified gold threads and microwires in three subsequent steps through the cyclic voltammetry (CV) method in a potassium ferricyanide $K_3[Fe(CN)_6]$ solution in a potential window of (−100 to + 450 mV) at different scan rates (10–300 mV s^{-1}). At step 1, we conducted cyclic voltammetry in 5 mmol L^{-1} of $K_4Fe(CN)_6$ bulk solution prepared in PBS (1×) in a three-electrode set up including a silver multifilament thread (15 mm length) as pseudo reference electrode and two gold multifilament (15 mm length) threads as counter electrodes in the case of unmodified and 6MCH-modified gold thread as the working electrodes. We employed silver microwire as a pseudo reference electrode (20 mm length) and 30 mm length gold microwire as a counter electrode in 5 mmol L^{-1} of $K_4Fe(CN)_6$ bulk solution in PBS (1×) to electrochemically study the unmodified and 6-MCH modified gold microwires. In step 2, we gently inserted the unmodified and 6MCH-modified gold threads and the microwires in a Coolmax-yarn while weaving the weave, which already included the aforementioned pseudo reference and counter electrodes in either case of the thread and the wire. To confine the liquid flow in the Coolmax wicking channels we used nail polish to stop the liquid at the other end of the perpendicular Coolmax yarns. We framed the Coolmax weave by weaving cotton yarns that do not wick and adsorb the liquid due to the layer of wax on the surface. By adding in a total 100 µL of 5 mmol L^{-1} $K_4Fe(CN)_6$ solution to the horizontal and vertical Coolmax wicking inlets, the redox solution wicked throughout the weave along and crossed the thread and wire-based electrodes; we conducted CVs by fixing the integrated fiber electrodes on plastic supports using the double-sided tape. As the last step, we took out the working electrodes gently from the weave and put them back in the bulk 5 mmol L^{-1} of $K_4Fe(CN)_6$ solution, and conducted CV using the mentioned three-electrode setup.

Design of Woven Microfluidic Device: We used a small portable weaving loom to weave and integrated the fiber electrodes in eight horizontal Coolmax wicking yarns in a way that each electrode was sandwiched between the four yarns as horizontal wicking channels. Also, there were three woven Coolmax wicking channels (three wicking yarns per channel) perpendicular to the fiber electrodes. We wove five strands of cotton yarns in the beginning and ending of the weave to frame the wicking yarns and used nail polish at the perpendicular Coolmax yarn to confine the liquid flow inside the weave, see Figure 2D,E, and Figure S11, Supporting Information.

Flexibility Characterization of Woven Microfluidic Device: We characterized the electrochemical performance of the thread and microwire electrode-based woven devices by fabricating them onto adhesive bandages and conducting the cyclic voltammetry technique in three different conditions including straight, 90 degree-bend, and folded form, as we were attached to a finger of a human subject, in presence of 5 mmol L^{-1} of potassium ferricyanide at 50 mV s^{-1} scan rate versus silver microwires/threads as pseudo-reference electrodes. We calculated the current density of both woven fiber electrodes in these three forms by normalizing the oxidation peak current of potassium ferricyanide in CV scans to the effective surface area of either of the fiber-electrodes. The human participant provided their informed, written consent to wear the device and be part of this study.

Scanning Electron Microscope (SEM): We conducted the SEM technique to characterize the structure and surfaces of the off-the-shelf, plasma coated gold threads, and the electropolished gold microwires, using a Hitachi Tabletop SEM TM-1000 (Japan).

RPA Basic Kit Primers and Stem-Loop Oligonucleotide Probe Design: We designed RPA Basic kit primers for SE_0105 gene of *S. epidermidis* ATCC 12228 to amplify 210 bp target amplicon and stem-loop (S-L) oligonucleotide probe, which was modified with methylene blue (MB) and hexamethylene thiol at 5′ and 3′ ends, respectively. The forward RPA primer was modified with a phosphate group at the 5′ end (Table 2) to convert double-stranded RPA target amplicon to ssDNA using lambda exonuclease enzyme for stem-loop DNA probe detection.

Tube-Based RPA Amplification, Making Single-Stranded DNA of RPA Products and Gel Electrophoresis: We carried out RPA basic kit amplification in 50 µL reaction volume, according to our previous report.[17] Briefly, we prepared a master mix, which contained 2.1 µL of 5′-phosphate modified-forward primer (8 µM), 2.1 µL of reverse primer (8 µM), 29.5 µL of rehydration buffer, and 8.2 µL of nuclease-free water to rehydrate freeze-dried RPA enzyme pellets and continued by adding 5 µL of 10 copies/µL purified genomic *S. epidermidis* DNA template as target samples and 5 µL of nuclease-free water as a blank sample. We initiated the RPA reaction with the addition of 2.5 µL of MgAc 240 mmol L^{-1} to the cap of the reaction tubes and placing the tubes in the PCR machine at 38 °C for 30 min. To make single-stranded target amplicons, we treated RPA products both target and blank samples each with a mixture of 1 µL of lambda exonuclease enzyme (1U) and 4 µL of the enzyme buffer provided in the enzyme kit for the whole 50 µL of reaction volume at 37 °C for 25 min and stopped the reaction by raising the temperature to 80 °C for 2 min. We visualized the RPA amplification product through gel electrophoresis using 3% Agarose gel in TBE (0.5×) buffer.

Fabrication of Microwire E-DNA Sensor: We fabricated the SAM-based stem-loop probe-modified gold microwire electrodes according to the previous literature reports.[17,29] Briefly, we cleaned gold microwire electrodes using the protocol mentioned in the SAM-modification of gold microwires experimental section. Then, we dried the electrochemically cleaned gold microwires using nitrogen gas and incubated in 1 µM reduced DNA probe (using 10 mmol L^{-1} of TCEP) in PBS (1×, pH 7.4) for 2 h at room temperature in the dark. To remove the physically adsorbed DNA probe from the gold electrode surface, we rinsed the electrodes thoroughly using MQ-water for 1 min and dried the microwire electrodes with nitrogen gas. Finally, we incubated the microwire electrodes in freshly prepared 2 mmol L^{-1} of 6-mercapto-1-hexanol solutions in PBS (1×, pH 7.4) for 4 h at room temperature in the dark. Afterward, we rinsed the excess 6-mercapto-1-hexanol using MQ-water for 2 min and stored the modified microwires in PBS (1×, pH 7.4) at 4 °C in the dark. Additionally, due to the slight light sensitivity of methylene blue and 6-mercapto-1-hexanol, they carried out all the main steps of gold microwire labeling in the dark.

Electrochemical Measurements of Microwire E-DNA Sensor Integrated into Woven Textile: Using Coolmax wicking and cotton yarns we wove the weave, with the same pattern described previously, to incorporate stem-loop DNA probe-modified gold microwire as a working electrode along with bare gold and silver microwires as counter and pseudo-reference electrodes, respectively. To measure the probe performance in the woven textile, we loaded 30 µL of the 250-fold diluted sample in PBS (1×) to each vertical and horizontal channels (in total 60 µL) and recorded cyclic voltammograms in a potential range of (−200 mV, +200 mV) at 50 mV s^{-1} scan rate and square wave voltammograms in the potential range (−200 mV, +200 mV) with 10 mV potential step, 20 mV amplitude, and 50 Hz frequency three-times after 5 min of hybridization time. We started with the addition of PBS (1×) and after 5 min, ran SWV to obtain baseline then drained the inlets using Kimwipe paper tissue and loaded either RPA blank sample treated with lambda enzyme or ssDNA RPA target, with an initial 10 copies/µL purified genomic DNA of *S. epidermidis*. We investigated four individual E-DNA sensors integrated into the woven textile for both lambda enzyme treated-RPA products: the RPA blank and the RPA target samples, by conducting SWV after 5 min of hybridization. We also characterized the response of six individual stem-loop DNA probe-labeled gold wires in the woven textile after a 5 min incubation with PBS (1×, pH 7.4). We measured the response of the E-DNA sensor using signal suppression $SS = (\Delta Ib - \Delta Iss) / \Delta Ib)$, in which ΔIb is the baseline peak current (in PBS 1×, pH 7.4) and ΔIss is the suppressed peak current in presence of the aforementioned samples. To prevent sample evaporation during the measurements, we covered the integrated woven textile using a plastic cover.

Statistical Analysis: We presented the experimental data as mean ± standard deviation (SD) for at least three independent samples ($n \geq 3$).

We normalized the SWV measurements to the lowest recorded current at each scan. Also, we calculated the current density of the woven fiber electrodes by normalizing the oxidation peak current of potassium ferricyanide at their respective CV scans to the effective surface area of either of the fiber-electrodes. We performed statistical analysis between two groups using Student's *t*-test (Two-Sample Assuming Unequal Variances) through Microsoft Excel 2016. The two-tailed $^{**}p$-value < 0.05 was considered statistically significant.

Supporting Information

Supporting Information is available from the Wiley Online Library or from the author.

Acknowledgements

This work was supported by the European Research Council (Grant 715268), and funding through the Knut and Alice Wallenberg Foundation.

Conflict of Interest

The authors declare no conflict of interest.

Data Availability Statement

Data available on request from the authors

Keywords

electrochemical biosensors, nucleic acid amplification tests (NAATs), recombinase polymerase amplification (RPA), self-assembled monolayers (SAMs), textile microfluidics

Received: January 7, 2021
Revised: March 14, 2021
Published online:

[1] a) E. Noviana, C. S. Henry, *Curr. Opin. Electrochem.* **2020**, *23*, 1. b) A. Nilghaz, D. R. Ballerini, W. Shen, *Biomicrofluidics* **2013**, *7*, 051501.
[2] a) R. S. Malon, L. Y. Heng, E. P. Córcoles, *Rev. Anal. Chem.* **2017**, 36. b) C. Carrell, A. Kava, M. Nguyen, R. Menger, Z. Munshi, Z. Call, M. Nussbaum, C. Henry, *Microelectron. Eng.* **2019**, *206*, 45. c) A. Ainla, M. P. Mousavi, M.-N. Tsaloglou, J. Redston, J. G. Bell, M. T. Fernández-Abedul, G. M. Whitesides, *Anal. Chem.* **2018**, *90*, 6240. d) T. Dong, G. A. Wang, F. Li, *Anal. Bioanal. Chem.* **2019**, *411*, 4401.
[3] a) R. H. Tang, L. N. Liu, S. F. Zhang, X. C. He, X. J. Li, F. Xu, Y. H. Ni, F. Li, *Microchim. Acta* **2019**, *186*, 521. b) Y. Xia, J. Si, Z. Li, *Biosens. Bioelectron.* **2016**, *77*, 774. c) S. Cinti, D. Moscone, F. Arduini, *Nat. Protoc.* **2019**, *14*, 2437.
[4] C. S. Wood, M. R. Thomas, J. Budd, T. P. Mashamba-Thompson, K. Herbst, D. Pillay, R. W. Peeling, A. M. Johnson, R. A. McKendry, M. M. Stevens, *Nature* **2019**, *566*, 467.
[5] M. R. de Eguilaz, L. R. Cumba, R. J. Forster, *Electrochem. Commun.* **2020**, *116*, 106762.
[6] a) J. Lu, S. Ge, L. Ge, M. Yan, J. Yu, *Electrochim. Acta* **2012**, *80*, 334. b) L. Wang, L. Wang, Y. Zhang, J. Pan, S. Li, X. Sun, B. Zhang, H. Peng, *Adv. Funct. Mater.* **2018**, *28*, 1804456.
[7] L. Wang, S. Xie, Z. Wang, F. Liu, Y. Yang, C. Tang, X. Wu, P. Liu, Y. Li, H. Saiyin, *Nat. Biomed. Eng.* **2020**, *4*, 159.
[8] P. Teengam, W. Siangproh, A. Tuantranont, C. S. Henry, T. Vilaivan, O. Chailapakul, *Anal. Chim. Acta* **2017**, *952*, 32.
[9] T.-E. Du, Y. Wang, Y. Zhang, T. Zhang, X. Mao, *Anal. Chim. Acta* **2015**, *861*, 69.
[10] a) J. C. Cunningham, N. J. Brenes, R. M. Crooks, *Anal. Chem.* **2014**, *86*, 6166. b) X. Li, K. Scida, R. M. Crooks, *Anal. Chem.* **2015**, *87*, 9009.
[11] S. Farajikhah, J. M. Cabot, P. C. Innis, B. Paull, G. Wallace, *ACS Comb. Sci.* **2019**, *21*, 229.
[12] S. E. Fosdick, M. J. Anderson, C. Renault, P. R. DeGregory, J. A. Loussaert, R. M. Crooks, *Anal. Chem.* **2014**, *86*, 3659.
[13] a) J. A. Adkins, C. S. Henry, *Anal. Chim. Acta* **2015**, *891*, 247. b) J. A. Adkins, E. Noviana, C. S. Henry, *Anal. Chem.* **2016**, *88*, 10639.
[14] X. Weng, Y. Kang, Q. Guo, B. Peng, H. Jiang, *Biosens. Bioelectron.* **2019**, *132*, 171.
[15] a) X. Mao, T.-E. Du, Y. Wang, L. Meng, *Biosens. Bioelectron.* **2015**, *65*, 390. b) I. Öberg Månsson, A. Piper, M. M. Hamedi, *Macromol. Biosci.* **2020**, *20*, 2000150. c) X. Li, J. Tian, W. Shen, *ACS Appl. Mater. Interfaces* **2010**, *2*, 1.
[16] C. Renault, X. Li, S. E. Fosdick, R. M. Crooks, *Anal. Chem.* **2013**, *85*, 7976.
[17] S. Khaliliazar, L. Ouyang, A. Piper, G. Chondrogiannis, M. Hanze, A. Herland, M. M. Hamedi, *ACS Omega* **2020**, *5*, 12103.
[18] R. Wang, Q. Zhai, T. An, S. Gong, W. Cheng, *Talanta* **2021**, *222*, 121484.
[19] M. Reches, K. A. Mirica, R. Dasgupta, M. D. Dickey, M. J. Butte, G. M. Whitesides, *ACS Appl. Mater. Interfaces* **2010**, *2*, 1722.
[20] J. C. Love, L. A. Estroff, J. K. Kriebel, R. G. Nuzzo, G. M. Whitesides, *Chem. Rev.* **2005**, *105*, 1103.
[21] A. James, J. Macdonald, *Expert Rev. Mol. Diagn.* **2015**, *15*, 1475.
[22] D. Corrigan, H. Schulze, G. Henihan, A. Hardie, I. Ciani, G. Giraud, J. Terry, A. Walton, R. Pethig, P. Ghazal, *Analyst* **2013**, *138*, 6997.
[23] M. Otto, *Nat. Rev. Microbiol.* **2009**, *7*, 555.
[24] B. S. Ferguson, S. F. Buchsbaum, J. S. Swensen, K. Hsieh, X. Lou, H. T. Soh, *Anal. Chem.* **2009**, *81*, 6503.
[25] a) B. Ma, J. Fang, W. Lin, X. Yu, C. Sun, M. Zhang, *Anal. Bioanal. Chem.* **2019**, *411*, 7451. b) X. Gao, X. Liu, Y. Zhang, Y. Wei, Y. Wang, *BMC Vet. Res.* **2020**, *16*, 130.
[26] L. Wang, X. Fu, J. He, X. Shi, T. Chen, P. Chen, B. Wang, H. Peng, *Adv. Mater.* **2020**, *32*, 1901971.
[27] a) A. Economou, C. Kokkinos, M. Prodromidis, *Lab Chip* **2018**, *18*, 1812. b) M. Tessarolo, I. Gualandi, B. Fraboni, *Adv. Mater. Technol.* **2018**, *3*, 1700310. c) A. Hatamie, S. Angizi, S. Kumar, C. M. Pandey, A. Simchi, M. Willander, B. D. Malhotra, *J. Electrochem. Soc.* **2020**, *167*, 037546.
[28] L. M. Fischer, M. Tenje, A. R. Heiskanen, N. Masuda, J. Castillo, A. Bentien, J. Émneus, M. H. Jakobsen, A. Boisen, *Microelectron. Eng.* **2009**, *86*, 1282.
[29] Y. Xiao, R. Y. Lai, K. W. Plaxco, *Nat. Protoc.* **2007**, *2*, 2875.